Crystallization in the Thin and Ultrathin Films of Poly(ethylene−vinyl acetate) and Linear Low-Density Polyethylene

Y. Wang,[†] S. Ge,[†] M. Rafailovich,*[,†] J. Sokolov,[†] Y. Zou,[‡] H. Ade,[‡] J. Lüning,[§] A. Lustiger,[⊥] and G. Maron[#]

Department of Materials Science and Engineering, State University of New York at Stony Brook, Stony Brook, New York 11794; Department of Physics, North Carolina State University, Raleigh, North Carolina 27695; Stanford Synchrotron Radiation Lab, Stanford, California 94209; ExxonMobil Research and Engineering Company, Annandale, New Jersey 08801; and Department of Applied Chemistry, The Hebrew University of Jerusalem, Jerusalem 91904, Israel

Received August 29, 2003

ABSTRACT: The crystallization of poly(ethylene−vinyl acetate) and linear low-density polyethylene (LLDPE) films spun-cast from the polymer/toluene solutions with as-cast thickness from 460 to 10 nm was studied. The lamellar thickness was measured using small-angle X-ray scattering (SAXS) and found to increase from 14 to 21 nm for films thinner than 100 nm. The morphology of LLDPE measured by scanning probe microscopy (SPM) showed an edge-on lamellae for the films thicker than 30 nm and flat-on lamellae for the films thinner than 15 nm. A pseudo-"shish-kebab" tiny crystal structure was observed in between the larger lamellae. Crystallinity was confirmed using attenuated total reflectance−Fourier transformed infrared spectroscopy (ATR-FTIR) and near-edge X-ray absorption fine structure (NEXAFS) spectroscopy. The shear modulation force microscopy technique (SMFM) was used to measure the melting point, T_m, which was found to decrease for films thinner than 100 nm. The rate of decrease was a function of the annealing protocol, but in all cases for films approximately 20 nm thick T_m was depressed by 35−40 °C. This large value cannot be predicted from the classical Gibbs−Thomson relation, unless a change in the effective heat of fusion is assumed due to surface interactions.

Introduction

Thin (thickness between 100 and 1000 nm) and ultrathin (thickness below 100 nm)[3] polymer films have received a great deal of attention recently due to their uses in the designing and engineering of electronic components where miniaturization is becoming increasingly important.[1−3] Studies of the behavior of polymers in confined spaces have demonstrated that the presence of interfaces greatly affects the conformation of chains,[4] segmental mobility,[5−7] viscoelastic properties,[8] and thermal transitions.[9−14] In semicrystal polymers, the picture is more complicated since one also has to consider the effects of the interface on the degree of crystallinity,[15,16] crystal growth rate,[15,17,18] morphology, and structure.[16,20−25]

Despotopoulou and co-workers[2,15,19] studied the crystallization of poly(di-*n*-hexylsilane) films ranging from 5 to 50 nm in thickness. They reported decreased crystallization dynamics and inhibition of microcrystallite formation in the restricted geometry of films thinner than 16 nm. Mellbring et al.[20] observed a change in morphology of spun-cast HDPE films from spherulite structure to aggregates of edge-on oriented lamellae when the film thickness is reduced to below 100 nm. Since the crystallization in this case occurred during spin-casting and solvent evaporation, the relationship of the observed structures to equilibrium ones was not established. Bartczak and co-workers[26] found a similar morphology change from spherulite to sheaflike aggregates in polyethylene thin films at a critical thickness of 400 nm. Schönherr et al.[16] imaged ultrathin PEO films crystallized on Si substrates and showed that for film thickness greater than 1000 nm the lamellae oriented edge-on, while in the films thinner than 300 nm the crystals were composed mostly of flat-on lamellae. Relatively few studies were reported for films thinner than 15 nm. Reiter et al. studied the morphology and growth mechanisms of PEO in quasi-two-dimensional crystals formed by fingering of the polymer at the edge of dewetting droplets where they found a high degree of crystallinity.[21−23] Similar phenomena were also reported by Taguchi et al.[25] and Sakai et al.[27,28] which determined the surface dynamics. Lovinger et al. observed single crystals grown from the melt of poly(trifluoroethylene) and discussed the morphology on the basis of the diffusion-limited aggregates.[29]

Despite the large number of studies on the morphology of the crystalline films, very few measurements exist on the effect of film thickness on the melting point. Kim et al.[30] measured the melting point, T_m, of EVA films as a function of thickness by observing the ellipsometric angles as a function of temperature. They found that T_m decreased when the sample thickness was below 30 nm. Since the ellipsometry did not have imaging capability, the morphology was not detected at the same time. Hence, it was not possible to determine whether the effect was due to entropic confinement of the lamellae or a decrease in the degree of crystallinity due to hindered dynamics near an attractive surface.

In this paper we demonstrate that by using scanning probe microscopy, we can measure both T_m and the morphology as a function of film thickness. Furthermore, by analyzing the samples with other complementary techniques, such as ATR-FTIR and NEXAFS

[†] State University of New York at Stony Brook.
[‡] North Carolina State University.
[§] Stanford Synchrotron Radiation Lab.
[⊥] ExxonMobil Research and Engineering Company.
[#] The Hebrew University of Jerusalem.
* Corresponding author: e-mail mrafailovich@otes.cc.sunysb.edu; phone (631)-632-8483.

10.1021/ma030456b CCC: $27.50 © 2004 American Chemical Society
Published on Web 04/01/2004

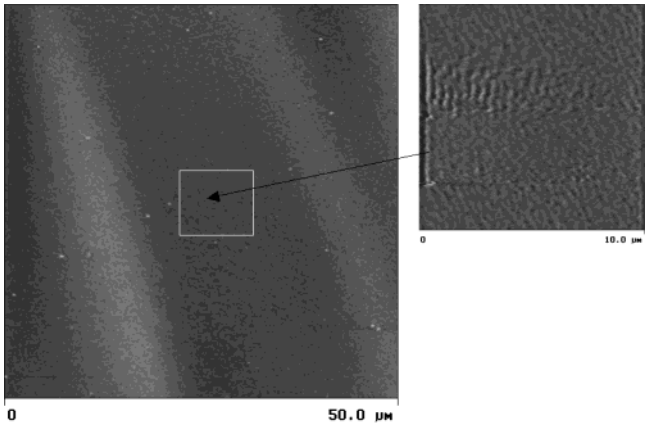

Figure 1. SPM height image of as-cast 15 nm thick film of LLDPE, which shows very uniform coverage on the Si substrate.

spectra, we can correlate changes in T_m with structural changes in the lamellae as well as the chain ordering. Since all these techniques are well-suited for thin films, we were able to study semicrystalline polymer films with thicknesses in the range of 460 nm to around 10 nm. The polymers we chose to study, poly(ethylene−vinyl acetate) (EVA) and linear low-density polyethylene (LLDPE), are all well-characterized materials for which the bulk crystallization parameters are known and can easily be compared to the thin film results.

Experimental Section

Preparation of Uniform Thin Films. The polymers used were poly(ethylene−vinyl acetate) purchased from Dupont Co. with the commercial name Elvax 770 (polydispersed random copolymer with 90.5 wt % ethylene, $T_m = 95$ °C) and the linear low-density polyethylene ($M_w = 50\,000$, $M_w/M_n = 2$, $\rho = 0.92$ g/cm^3, $T_m = 117$ °C), which is an experimental material provided by ExxonMobil Chemical with hexane as the comonomer, polymerized using metallocene catalysis. The polymers were dissolved in toluene, and the solution was heated to approximately 150 °C to ensure complete dissolving.

Si(111) substrates were prepared by boiling the wafers in a mixture of $H_2SO_4/H_2O_2/H_2O$ (1:1:3 in volume) for 1 h at 150 °C, rinsed with deionized water, and etched in HF/H_2O (1:8 in volume) solution for 20 s right before spin-casting, which rendered the surface hydrophobic. Ge prisms were used solely as the substrates for the FTIR samples.

The substrates were then heated to 150 °C, and the hot polymer solution was spun-cast onto the heated substrates. The procedure was necessary to prevent the films from immediately crystallizing on the substrate and dewetting the Si wafers. The thickness of the films was controlled by varying the concentration of the polymer solution (0.05−5 wt %) while fixing the rotation speed of the substrate at 2500 rpm. Uniform thin films could be prepared in this manner, and the as-cast thicknesses, ranging from 10 to 460 nm, were measured using a three-wavelength AutoEL-II ellipsometer (Rudolf Research). The uniformity of the films was examined using scanning force microscopy both before and after annealing. A typical large-scale image of the LLDPE film of 15 nm thick, before annealing, is shown in Figure 1, where one can see that even for the thinnest films the thickness is uniform and the Si surface is completely covered by polymer. Smaller scale scans, such as the one shown on the right, were taken at many places on the sample and found to be similar.

Two crystallization conditions were used. The first, nonisothermal crystallization, consisted of heating the films in a vacuum of 10^{-3} Torr in an oil trapped vacuum oven (Hotpack Co.) at elevated temperatures (120 °C for EVA and 140 °C for LLDPE) for 30 min, which was sufficient to melt the films and remove the previous thermal history; the temperature was then decreased gradually to room temperature over a period of 12 h before exposing the samples to the atmosphere. (Note: all the experimental results in the following section that are not specified thermal history were under nonisothermal crystallization.) The second is the isothermal condition (for LLDPE), in which the films were first annealed well above T_m at 140 °C for 30 min and then quickly moved to another vacuum oven set at 60 °C, where they were further annealed for 12 h before exposure to room temperature.

The TEM samples were made by floating the films off the substrate in a KOH/water solution, maintained at 60 °C. KOH dissolves the native SiO_x layer on silicon wafers, without affecting the hydrophobic polymer film. This allows the polymer films to be floated onto carbon/Formvar-coated Cu mesh TEM grids.

Imaging. The topography of the films was imaged using a Digital Instruments Dimension 3000 scanning probe microscope (SPM) in the contact mode using a Si_3N_4 tip. More detailed structure was imaged with the Philip CM12 transmission electron microscope operated at the voltage of 120 kV.

Small-Angle X-ray Scattering. Small-angle X-ray scattering (SAXS) for EVA films was carried out at the Brookhaven National Laboratory National Synchrotron Light Source on beamline X27C with an X-ray wavelength of 0.1309 nm.

Measurement of Crystallinity. *(A) Attenuated Total Reflectance−Fourier Transformed Infrared Spectroscopy (ATR-FTIR).* Spectra were recorded using a Nicolet 760 FTIR unit equipped with an MCT detector cooled with liquid nitrogen. A total of 2000 scans were taken for each spectrum at 2 cm^{-1} resolution.

(B) Near-Edge X-ray Absorption Fine Structure Spectra (NEXAFS). It has been previously demonstrated[31] for bulk polyethylene copolymers that the C−H doublet[32] at 287.6 and 288.2 eV is very sensitive on the crystallinity of the films. Either increase of branching ratio or melting makes the higher energy peak lose its intensity; in the meantime, the C−C σ^* features in the range between 290 and 295 eV blur out. These can serve as a further criterion for judging the crystallinity in current polyethylene films. The present NEXAFS experiments have been carried out at beamline BL-5-2 at the Standford Synchrotron Radiation Laboratory with total electron yield (TEY) mode. The beam spot was defocused to about 2 mm by 2 mm in order to avoid any radiation damage.

Measurement of the Melting Point. Shear modulation force microscopy (SMFM)[33] was employed to measure the melting temperature of the film on a local scale. The measurements were made using a Digital Instruments Dimension 3000 located in a sealed glovebox purged with dry nitrogen. Samples were mounted on an MMR Technologies heating/cooling stage which was calibrated by determining the melting point of naphthalene (353.3 K) and indium (429.7 K) crystals. In this method, a sinusoidal drive signal with a frequency of 1400 Hz was applied to the X-piezo controlling the cantilever, inducing a small oscillatory motion of the tip parallel to the sample surface. A normal force of 25 nN is applied to the tip which produces an indentation, h, into the sample. The lateral deflection amplitude Δx was measured as the output.

It was concluded from the previous experiments[33,34] that the increase in the tip penetration, h, as the polymer softens leads to a larger lateral deflection, Δx.

The indentation of the tip according to Hertz model[35] is

$$h = \left[D\frac{L}{R^{1/2}}\right]^{2/3}, \quad D = \frac{3}{4}\frac{1-\nu^2}{E}, \quad E = 2(1+\nu)G \qquad (1)$$

where R is the tip radius, L is the load applied to the tip, E and G are Young's modulus and shear modulus, respectively, and ν is Poisson's ratio.

On a given sample, G changes abruptly by more than 3 orders of magnitude at $T = T_m$. This results in an abrupt increase in the penetration depth of the tip and thus an abrupt increase in the amplitude of the tip deflection, Δx. The melting point can then be determined by slowly (1.0 °C/min) increasing

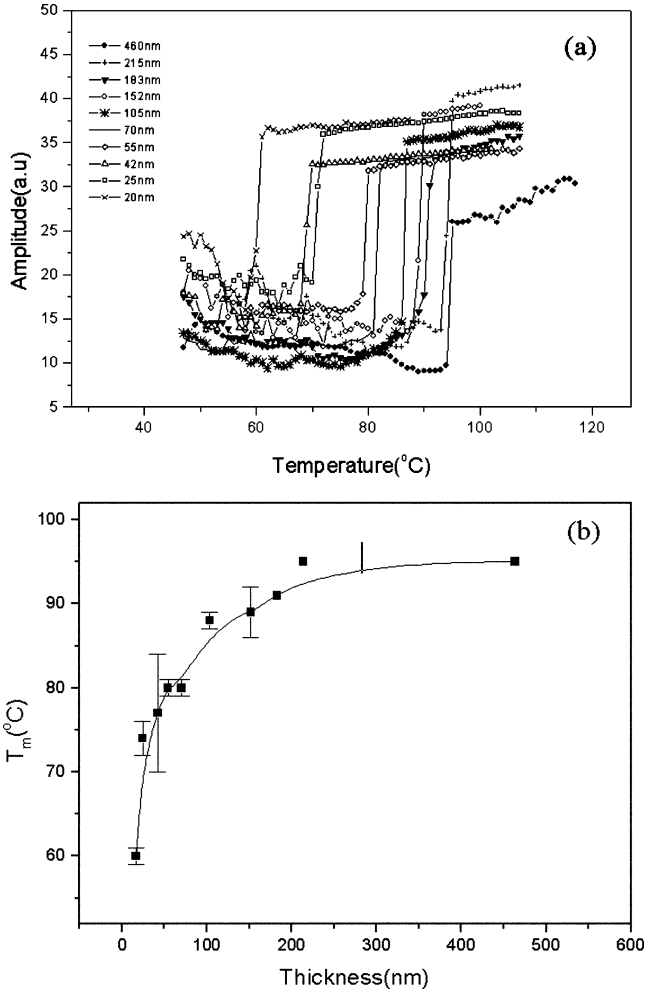

Figure 2. T_m dependence on the film thickness for EVA films. (a) Original curves of amplitude vs temperature for different film. The temperature where the amplitude abruptly increases is the melting point. (b) Summary of the T_m as a function of the film thickness.

the temperature of the sample heating stage from room temperature to 145 °C while recording Δx.

Results

Melting Temperature Depression in the Thin Films of EVA. The amplitude, Δx, vs temperature curves for EVA films of different thickness ranging from 460 to 20 nm as measured by the SMFM method are shown in Figure 2a.

From the figure we can see that all the curves have an abrupt transition which occurs within 2 deg. The values of the T_m extracted from these curves for different film thicknesses were plotted in Figure 2b. From Figure 2b we find that for films thicker than 200 nm T_m is exactly the same as the bulk value (95 °C), as measured by DSC. A very slow rate of decrease in T_m becomes measurable as the film thickness decreases beyond 150 nm. This is followed by a relatively large rate of decrease when the thickness falls below 70 nm. In the thinnest films (20 nm) we find that T_m is reduced by 35 deg or $T_m = 60$ °C. Kim et al.[30] also reported a decrease in T_m. In their case though, the decrease was only 15 deg for EVA and appeared to occur more abruptly at lower (30 nm) film thickness. On the other hand, since their polymer had a much higher vinyl acetate content, 25% vs 9.5% in the EVA in this study,

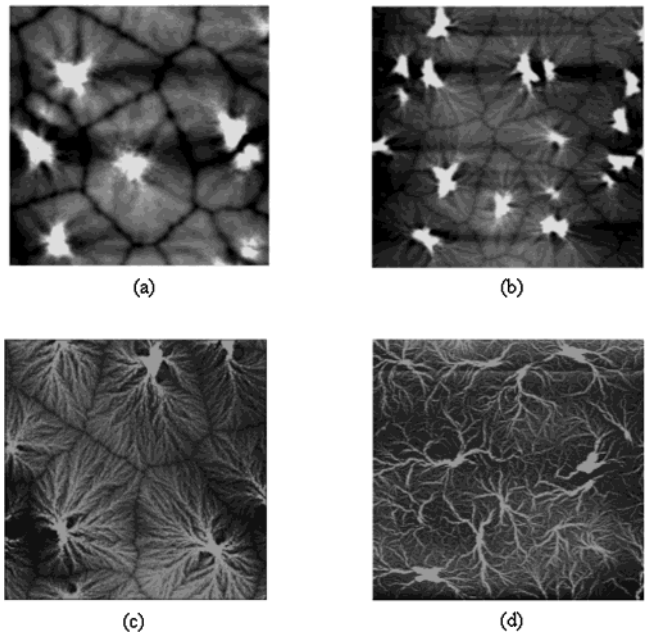

Figure 3. SPM height images of the EVA films with thickness: (a) 460, (b) 152, (c) 70, and (d) 20 nm. Scan size: 50 μm.

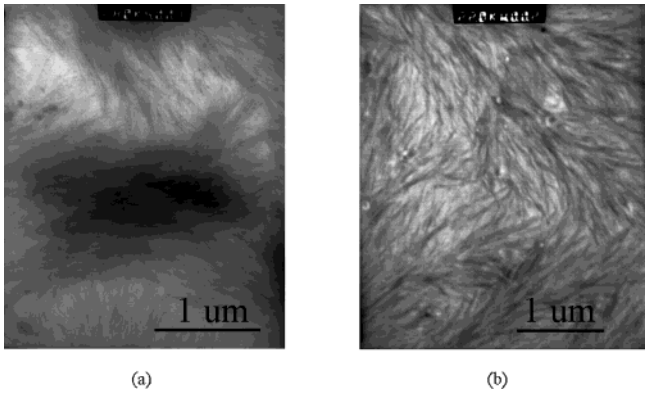

Figure 4. TEM images of the film with thickness: (a) 152 and (b) 35 nm.

we cannot compare the actual values of T_m and can only conclude that qualitative agreement exists.

Kim et al.[30] speculated that the decrease was due to decreased dynamics near the surface, which hindered crystallization of the polymer. We therefore imaged the films in order to determine the crystalline structure and see whether an increase in disorder can be observed with the onset of the decrease in T_m.

The scanning probe topographical images of films of different thickness are shown in Figure 3, and the corresponding TEM images are shown in Figure 4. From the figures we see that film of 460 nm thickness is bulklike and shows a compact spherulite structure with a large well-defined nucleus and small lamellae. As the film thickness decreases to approximately 70 nm, the packing of the spherulites becomes more open and the lamellae gradually increase in size. For films thinner than 70 nm, the spherulite boundaries disappear, and large lamellae appear to have originated from more nucleation centers, until for the thinnest films we have only very sparse hedrites. The detailed structure of the crystals is seen more clearly in the TEM images shown in Figure 4. Here, one can see that the thickness of the lamellae is much smaller in the thicker films (152 nm) than in the thinner film (35 nm). Since twisting or

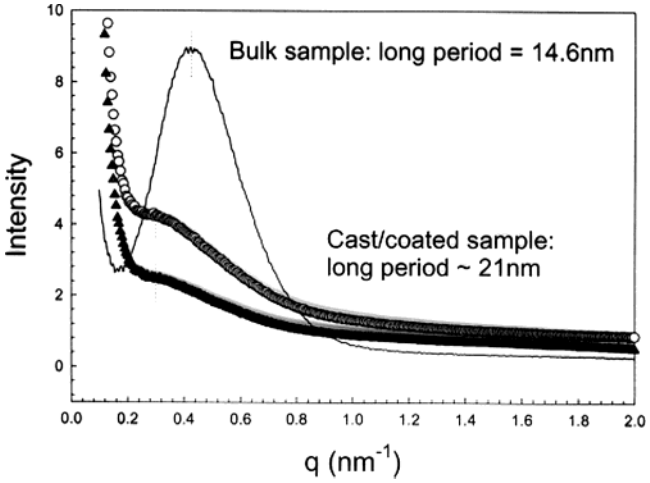

Figure 5. Small-angle X-ray scattering of the EVA bulk material and spin-coated films of 35 and 50 nm.

tilting of the lamella makes it difficult to determine the lamellar spacing from the images unless the tilt angles are known, small-angle X-ray scattering was performed to measure the lamellar thickness. The results are shown in Figure 5, for two films, 35 and 50 nm thick together with a bulk sample (solid line). From the scattering peaks observed in the figure we find that the long period for the bulk material is 14 nm while that of both thin films is 21 nm. These results suggest that the lamellar thickness increases rather than decreases, with film thickness decrease.

Classically T_m is related to the lamellar thickness according to the Thomson−Gibbs equation:[36,37]

$$T_m = T_m^0 - \frac{2\gamma_e T_m^0}{l\Delta H_v} \qquad (2)$$

Here T_m^0 is the melting point for the infinitely large crystal, γ_e is the top and bottom surface energy of the crystal lamellae, ΔH_v is the heat of fusion, and l is the lamellae thickness. Since l in fact increases rather than decreases with films thickness, hence the T_m depression cannot be attributed to the l decrease as was usually assumed.

Since EVA is a random copolymer, the structure of the crystallites as the film thickness decreases may reflect the preferred absorption of the acetate at the Si substrate surface, rather than an intrinsic property of surface-induced crystallization. Furthermore, since the acetate component is amorphous, it may swell the crystalline fibrils, further complicating the interpretation. To obtain a more quantitative analysis, we therefore decided to perform these experiments on films of linear low-density polyethylene homopolymer which are better characterized.

LLDPE. 1. Morphology. The SPM images of polyethylene with the as-cast thickness ranging from 250 to 15 nm, crystallized in nonisothermal condition, are shown in Figure 6. For each films of each thickness, two images were shown. The left is the height image with a scan size of 50 μm, and the right is the lateral force image with a scan size of 5 μm.

From the figure we can see that for films 250 nm thick the crystals grow as typical spherulites, with well-defined nuclei from which the crystalline lamellae fan out to fill up the volume of the film. It is interesting to note that the films appear to have a granular morphology. As the film thickness decreases from 70 to 30 nm, the spherulitic features are still obvious, but the crystal aggregates are more open. These structures are highly reminiscent of the open spherulitic structures shown by Keith and Padden[38] during crystallization of an isotactic polypropylene blend with a high concentration of atactic polypropylene. As the film thickness decreases further to 15 and 10 nm (morphologies of these two films are very similar; the image of 10 nm is not shown here), the crystals appear to grow in a dendrite-like shape, with more isolated parts.

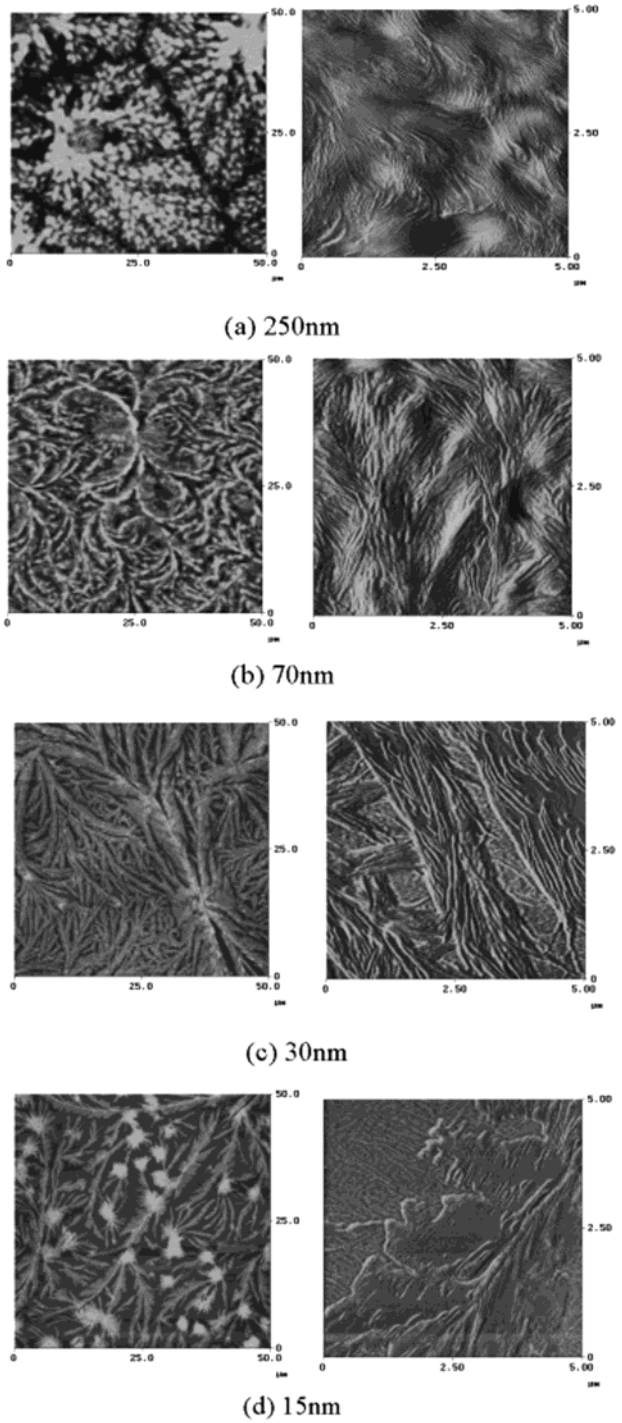

Figure 6. SPM images of the LLDPE films with thicknesses ranging from 250 to 15 nm crystallized nonisothermally. In each figure, the left is the height image with scan size of 50 μm, and the right is the friction image with a scan size of 5 μm.

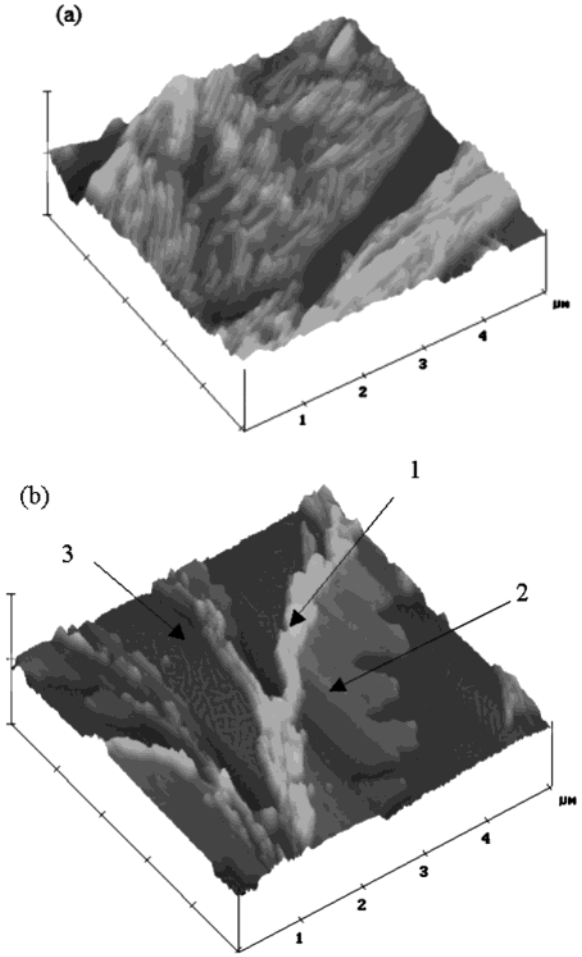

Figure 7. 3-D view of the films with thickness: (a) 30 and (b) 15 nm. Region 1: "ridge" area with edge-on lamellae; region 2: flat-on lamellae; region 3: pseudo-"shish-kebab" tiny crystal.

A more detailed view of the lamellae structure of the films can be seen from the lateral force images. In these images the crystalline structures appear darker since they are harder, and the tip deflection is less than in the softer amorphous regions where the tip penetrates more deeply. The increased contact area results in a larger lateral deflection and hence softer regions appear brighter. From the figure we can see that the 250 nm film has a well-organized lamella structure, oriented edge-on with respect to the film surface. For the film that is 70 nm thick, the lamellae still organize into sheaflike aggregates, but the aggregates are separated farther apart from each other. The size of the lamellae appears greater. This apparent increase may be due to either an actual increase in the lamellar thickness or a tilt of the lamellae from the perpendicular orientation caused by loose packing. In the 30 nm thick film a less well-organized lamellae aggregation is observed with a still larger gap between the lamellae. As the film thickness is further decreases below 15 nm, a large part of the crystal shows a rather flat surface, the height of which is approximately 10−15 nm, which is the typical value of the lamellar thickness of a single crystal.

To better identify the orientation of the lamellae, the 3D view of the height images of 30 and 15 nm films are shown in Figure 7.

In the 30 nm film most lamellae take a nearly perpendicular orientation to the surface while, in the 15 nm film flat crystals (designated as region 2) grow in the periphery of the edge-on lamellae region (region 1). These large flat lamellae are separated by even flatter spaces (region 3). The question then arises as to what is the nature of the material between the lamellae—is it a thin film of amorphous polymer which is immobilized by adsorption to the surface, or is it bare Si? Or is the film dewetting the surface by forming an incomplete layer, exactly one lamella high in a manner analogous to the islands formed in partial layers of lamellar block copolymers?[39]

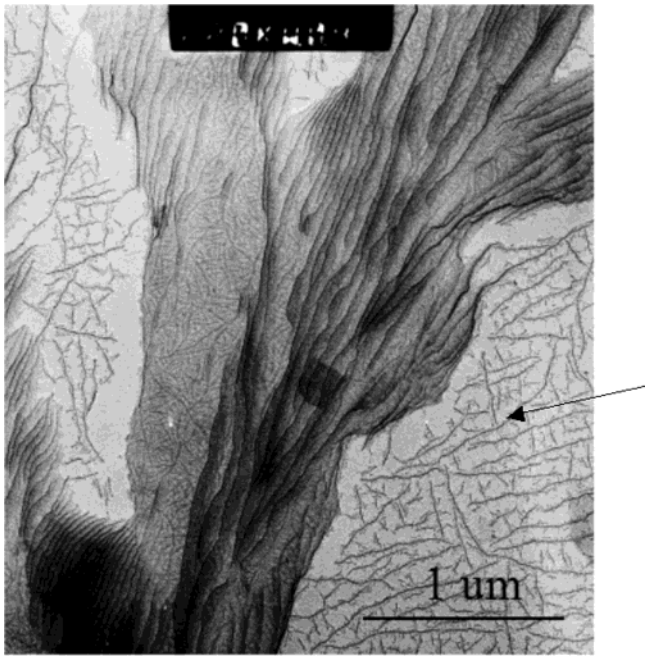

Figure 8. TEM image of the LLDPE film of 15 nm thick.

To obtain a more detailed view of this area, the films were lifted from the Si surface onto TEM grids, and the TEM images of a 15 nm film are shown in Figure 8. From the figure we can clearly see that the region between lamellar islands is covered by polymer. This is consistent with the empirical observation that the films did not disintegrate upon liftoff as was expected if these regions were bare silicon. Furthermore, from the figure we find that this layer is not amorphous, but rather composed of a uniform network of very small crystals with large-angle branching, as pointed by the arrow. This structure looks very similar to the "shish-kebab" crystals which are usually formed under stress. Since this layer is much thinner than the natural lamellar height, the actual crystal structure is unknown, and the comparison can only be qualitative. On the other hand, since the chains are stretched thinner than their normal configuration due to surface interactions, it would not be surprising if large stresses existed in this layer.

2. Crystallinity Measurement. The existence of crystallinity cannot be confirmed solely from morphology. In particular, since the very small pseudo-"shish-kebab" structures cover large areas of the film surface, it was important to confirm that they were indeed crystalline by other techniques, such as FTIR and NEXAFS, which offer a more direct measure of crystal ordering than SPM. In polyethylene, splitting of the CH_2 rocking band is an indication of the presence of crystallinity.[40,41] In the amorphous state, the rocking band is a broad band centered at 723 cm^{-1}. However, in crystal state, the band splits into two narrow bands located at 730 and 720 cm^{-1}. Figure 9 shows the FTIR spectra of

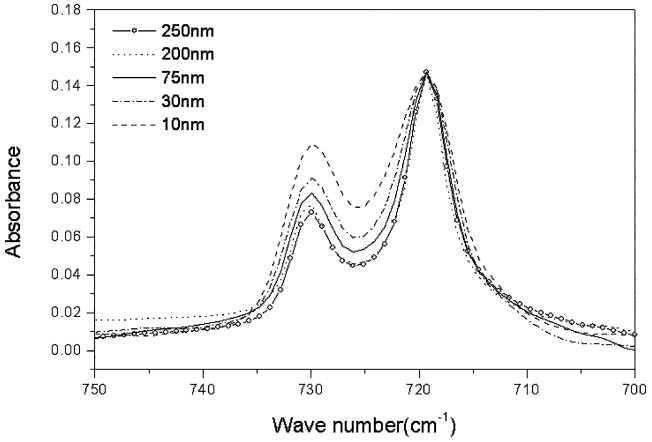

Figure 9. ATR-FTIR spectrum of the LLDPE films with different thickness.

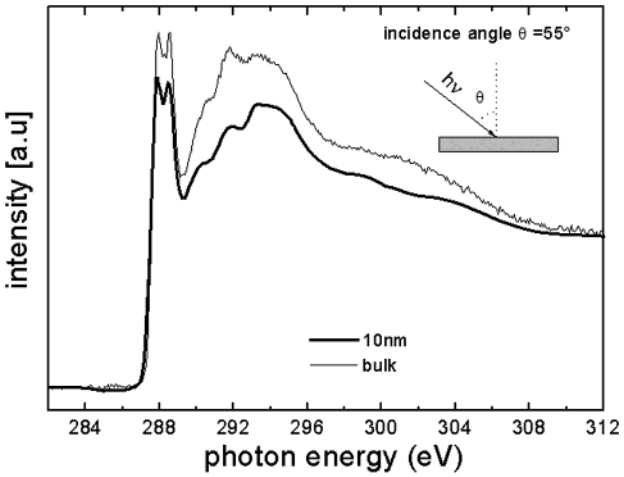

Figure 10. NEXAFS curves for the LLDPE bulk material and the film of 10 nm thick.

LLDPE crystallized nonisothermally. All the spectra are normalized to full scale; thus, the intensity is not affected by the film thickness. From the figure we can see that the splitting of the rocking band located at 730 and 720 cm^{-1} is obvious for the film as thin as 10 nm, which indicates that the films are crystalline for all thicknesses, which is in agreement with the TEM micrographs and confirms that the tiny network structure observed is some form of crystalline structure.

Crystallinity was further confirmed in Figure 10, which shows the NEXAFS spectra from a bulk LLDPE sample and a thin (10 nm) film measured at an incidence angle of 55°.

Both spectra consist of a C−H doublet and C−C σ^* features. As revealed in ref 31, a least decrease of crystallinity from 45% to 35% will result in an obvious decrease of the intensity of second peak of doublet. The fact that in the ultrathin film with a thickness as 10 nm the C−H doublet persists, along with clearly identifiable C−C fine σ^* features, is a clear evidence for the existence of crystallinity.

3. Melting Temperature Depression. The amplitude vs modulation curves for LLDPE films of different thicknesses are shown in Figure 11 for films crystallized both (a) nonisothermally and (b) isothermally at 60 °C. As discussed previously, the discontinuity in amplitude corresponds to the melting point of the sample and was plotted as a function of film thickness in Figure 12.

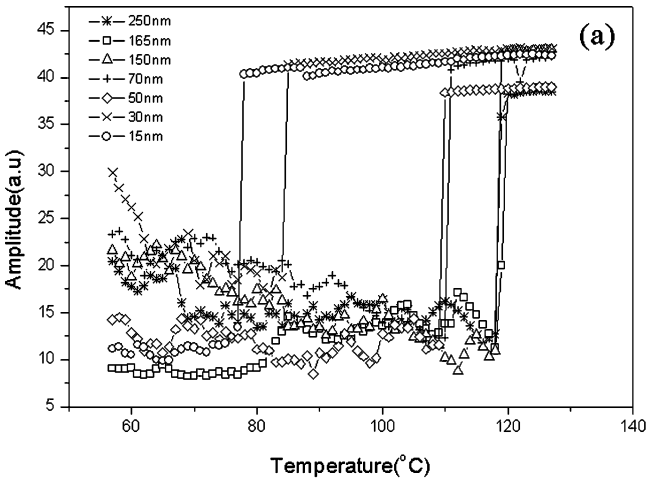

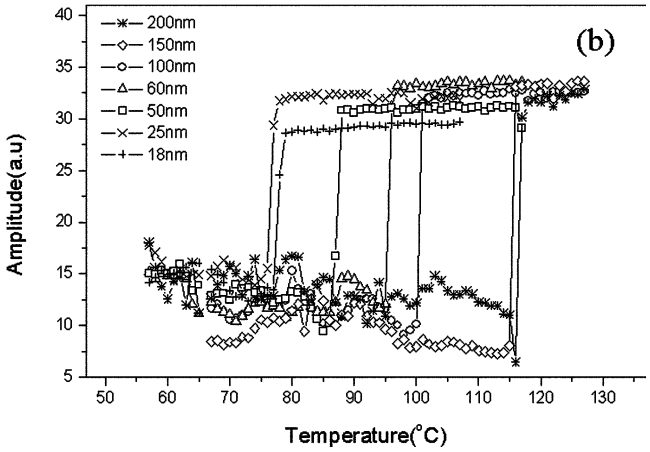

Figure 11. Original curves of amplitude vs temperature for the LLDPE films: (a) nonisothermal crystallization; (b) crystallization at 60 °C.

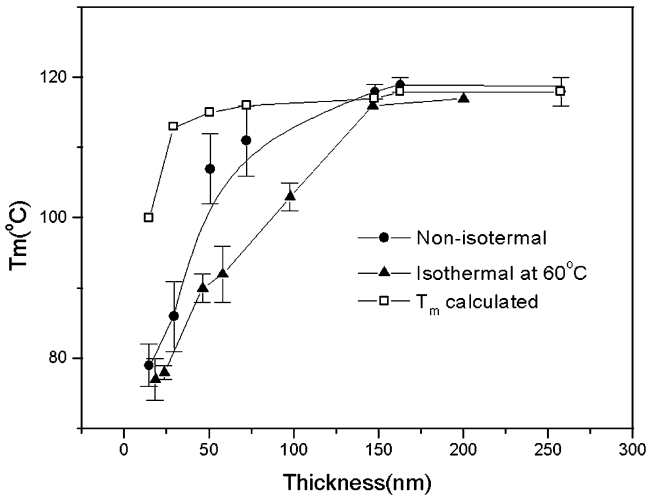

Figure 12. Summary of the melting point dependence on the film thickness for the LLDPE films.

At least five pieces for each film were tested, and the points shown in the figure correspond to the average value. From Figure 7b we can see that on the surface of films thinner than 20 nm three different types of morphologies are observed. Since each region may have different melting points, care was taken to position the tip only on the region of interest, which in this case were the large flat lamellae. This was accomplished by first scanning the morphology of $10 \times 10\ \mu m^2$ area, selecting the area of interest by offsetting and then stationing

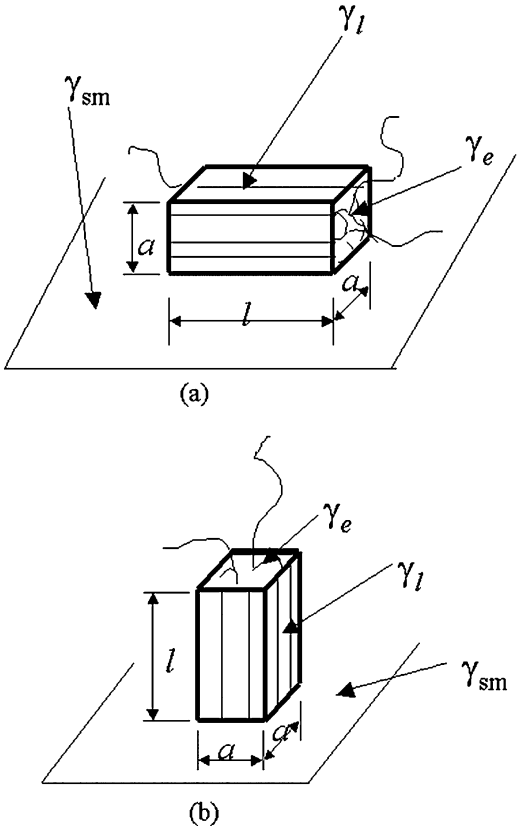

Figure 13. Two contact ways of the primary nucleus with respect to the substrate: (a) chain parallel to the substrate, lamellae edge-on; (b) chain perpendicular to the substrate, lamellae flat-on.

the tip at the center of the scan for the T_m measurement. For all the films tested, the error in T_m was less than 5 deg. From Figure 12 we can see that for all films greater than 150 nm T_m = 117 °C or is the same as the bulk value. As the film thickness decreased below 150 nm, an abrupt, almost linear, decrease in T_m with thickness is observed in the samples crystallized under isothermal conditions. In the nonisothermal crystallized films, the decrease is initially more gradual, but the slopes of the two curves appear parallel for films thinner than 50 nm. Both curves intersect at a nominal spun-cast thickness of 15 nm, where T_m is 79 °C, which is 38 °C lower than that of the bulk material. The intersection may be due to the fact that in both cases we are sensing a film only one lamellae in height, and the simple structure of the film makes it less sensitive to the annealing protocol.

Discussion

It has previously been observed that surface interactions are very efficient at orienting crystalline films.[20,26] The preference of edge-on orientation of lamellae can be seen directly from minimization of the energy for the primary nucleation step. To calculate the critical energy of the primary nucleus, we follow the derivation by Wunderlich[36] modified with additional terms to account for the surface interactions.

As shown in Figure 13, assume the primary nucleus is of size $a \times a \times l$, where l is the size of the primary nuclei along the chain direction and a is that at the folded direction. Two possible contact ways of the primary nucleus with the substrate are shown in Figure 13. Part a is the way that the chain parallel to the substrate, i.e., subsequent growth of the crystal in the same orientation, will lead to edge-on lamellae. Part b is chain perpendicular to the substrate, and the subsequent growth of the crystal in the same orientation will lead to flat-on lamellae.

In case a, the free energy change in the formation of nucleus is

$$\Delta G = -a^2 l \Delta G_v + 2a^2 \gamma_e + 3al\gamma_l + al(\gamma_{cs} - \gamma_{ms}) \quad (3)$$

From

$$\partial \Delta G/\partial a = 0, \quad \partial \Delta G/\partial l = 0 \quad (4)$$

We get the critical nucleus size

$$a^* = \frac{3\gamma_l + \gamma_{cs} - \gamma_{ms}}{\Delta G_v}, \quad l^* = \frac{4\gamma_e}{\Delta G_v} \quad (5)$$

In case b

$$\Delta G = -a^2 l \Delta G_v + 4al\gamma_l + a^2(\gamma_e + \gamma_{cs} - \gamma_{ms}) \quad (6)$$

From the same derivation, we got

$$a^* = \frac{4\gamma_l}{\Delta G_v}, \quad l^* = \frac{2(\gamma_e + \gamma_{cs} - \gamma_{ms})}{\Delta G_v} \quad (7)$$

Here, ΔG_v is the free energy change on crystallization per unit volume, $\Delta G_v = \Delta H_v \Delta T/T_m^0$, γ_e is the interfacial energy between the folding plane of the crystal and the polymer melt, and γ_l is that between the lateral plane and the melt. γ_{cs} is the interfacial energy between the crystal and the substrate, and γ_{ms} is that between the melt and the substrate.

Since γ_e is far greater than γ_l ($\gamma_e = 93 \pm 8$ erg/cm^2, γ_l = 10−15 erg/cm^2)[42] and the crystal favors the contact with the substrate, so that $\gamma_{cs} < \gamma_{ms}$, we have

$$\gamma_{cs} - \gamma_{ms} < 0 < \gamma_l \ll \gamma_e \quad (8)$$

If we take γ_e = 100 erg/cm^2 (10^{-5} J/cm^2), γ_l = 10 erg/cm^2 (10^{-6} J/cm^2), ΔH = 50 cal/cm^3 (209 J/cm^3),[36] ΔT = 60 K, T_m^0 = 400 K, and assume $\gamma_{cs} - \gamma_{ms}$ to be 0, −10 erg/cm^2 (10^{-6} J/cm^2) and −20 erg/cm^2 (2×10^{-6} J/cm^2), respectively, and calculate the ΔG^* in these three different values, we got when $\gamma_{cs} - \gamma_{ms} = 0$ ΔG^* is approximately 170×10^{-21} J for both case a and b; when $\gamma_{cs} - \gamma_{ms} = -10$ erg/cm^2 (10^{-6} J/cm^2), in case a ΔG^* = 0 while in case b $\Delta G^* = 146.5 \times 10^{-21}$ J; for $\gamma_{cs} - \gamma_{ms}$ = −20 erg/cm^2 (2×10^{-6} J/cm^2), $\Delta G^* = -714.6 \times 10^{-21}$ J in case a and $\Delta G^* = 130.2 \times 10^{-21}$J in case b. So as long as $\gamma_{cs} - \gamma_{ms} < 0$, the critical energy of nucleation is much lower in case a than in case b. Thus, the primary nuclei favor the orientation in case a and chain parallel to the substrate. When the film is thick, the secondary nucleation and the subsequent growth of the crystals are more likely to take the same orientation as that of the primary nuclei so as to minimize the new interface area increase and thus the interfacial energy increase, resulting in the well-organized edge-on lamellae. However, when the film is very thin, the edge-on lamellae would create far more interface areas than the continuous flat ones, as shown in Figure 14, which is not thermodynamically favored. As can be seen from the SPM images (Figure 7b), apart from the few edge-on ridge areas (region 1), a large part of the lamellae are flat. The edge-on lamellae still take the primary nucle-

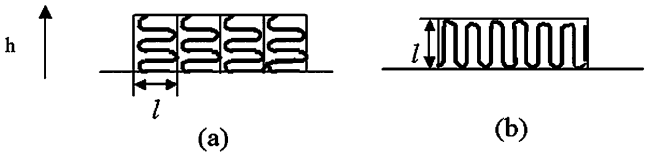

Figure 14. Lamellae orientation in the ultrathin films: (a) lamellae perpendicular to the substrate, a lot of interfaces created; (b) lamellae flat-on with respect to the substrate, interfacial areas substantially reduced.

ation controlled orientation, and the flat-on lamellae always grow in contact with the edge-on ones. Thus, the growth of these lamellae can be viewed as the result of secondary nucleation and crystal growth on the basis of the "ridge" lamellae. For the purpose of minimization of the interface energy, they no longer grow in the same direction as their primary nuclei; instead, they grow in the form of continuous flat crystals.

We can now try to estimate the change in T_m predicted from the Thomson−Gibbs equation. Let us first look at the thermodynamic basis of melting.

The overall change in free energy on melting is

$$\Delta G = xyl\Delta G_v - 2l(x + y)\gamma_l - 2xy\gamma_e \qquad (9)$$

Since

$$\Delta G_v = \Delta H_v \Delta T/T_m^0, \quad \Delta T = T_m^0 - T \qquad (10)$$

The melting point can be directly related to the lamellar size by combining eqs 9 and 10, and we obtain

$$T_m = T_m^0 - \frac{2\gamma_e T_m^0}{l\Delta H_v} - \frac{2\gamma_l}{\Delta H_v}\left(\frac{1}{x} + \frac{1}{y}\right)T_m^0 \qquad (11)$$

where ΔG_v, γ_e, γ_l, ΔH_v, and T_m^0 have the same physical meaning as in eqs 2 and 3; x, y, and l are width, length, and thickness of the lamella, respectively.

In bulk materials, the x and y are orders of magnitude larger than l, so the last two terms in the equation are relatively small and can be neglected. This then yields the well-known form of the Thomson−Gibbs equation, which is eq 2. In the thin films, the $y \gg x \sim l$, and hence second term should also be included.

Hence, for the thin film case

$$T_m = T_m^0\left(1 - \frac{2\gamma_e}{l\Delta H} - \frac{2\gamma_l}{x\Delta H}\right) \qquad (12)$$

Taking the values used above, the bulk values of l, surface energy of 36.2×10^{-3} N/m for γ_l,[43] T_m^0 was calculated to be 398.2 K. The T_m for different film thickness was calculated and plotted in Figure 13, from which we can see that the T_m depression is much smaller than the measured values. Furthermore, if we insert the measured values of l of the thin films, which is larger than the bulk value, the calculated depression is even smaller. Thus, the geometric confinement alone cannot explain the observed sharp decrease of T_m. Instead, T_m depression may be attributed to the intrinsic property change of the polymer near the substrate. For example, it is possible that the melting point depression indicates a change in the effective ΔH, where an additional term may have to be considered to account for desorbtion of the polymer chains from the surface. When the chains are pinned by an attractive surface, desorption must first occur in order for them to diffuse into the crystallizing region. If this is the case, then we would predict that the depression of T_m would be a function of the interactions between the polymer and the substrate. Further work is in progress to probe this hypothesis where we are modifying the surface with different coatings.

Conclusions

EVA and LLDPE films were prepared by spin-casting with thickness ranging from 460 to 10 nm. A large degree of crystallinity was observed even for films as thin as 10 nm, which could be attributed to surface-induced crystallization; as in the ultrathin films, very small crystals with large angle branching could be observed between the lamellae. The crystal morphology was also observed to have a strong dependence on film thickness. Films thicker than 200 nm exhibited spherulitic crystal morphologies with densely packed lamellae. As the film thickness decreased below 70 nm, the packing became less dense and large open structures were present. In films thinner than 15 nm, a single layer of flat crystal was observed. The melting point was measured and found to decrease with decreasing thickness for films thinner than approximately 100 nm for both EVA and LLDPE polymers. Since the lamellae thickness in fact increases rather than decreases with film thickness, geometric confinement alone cannot account for the large drop in T_m. To explain the depression, we postulate that an additional term in Thomson−Gibbs equation must be considered in order to account for the polymer−surface interactions besides the interfacial energy.

Acknowledgment. Support from the NSF (DMR-6080604) is gratefully acknowledged.

References and Notes

(1) Bartczak, Z.; Argon, A. S.; Cogen, R. E.; Weinberg, M. *Polymer* **1999**, *40*, 2331.
(2) Frank, C. W.; Rao, V.; Despotopoulou, M. M.; Pease, R. F. W.; Hinsberg, W. D.; Miller, R. D.; Rabolt, J. F. *Science* **1996**, *273*, 912.
(3) Feng, X.; Razavi, B.; Xu, H.; Cheng, Z. Y.; Zhang, Q. M. *J. Appl. Phys.* **2002**, *92*, 3111.
(4) Kraus, J.; Muller-Buschbaum, P.; Kuhlmann, T. *Europhys. Lett.* **2000**, *49*, 210.
(5) Zheng, X.; Sauer, B. B.; Alsten, J. G. V.; Schwartz, S. A.; Rafailovich, M. H.; Sokolov, J.; Rubinstein, M. *Phys. Rev. Lett.* **1995**, *74*, 407.
(6) Zheng, X.; Rafailovich, M. H.; Sokolov, J.; Strzhemechny, S.; Schwarz, S. A.; Sauer, B. B.; Rubinstein, M. *Phys. Rev. Lett.* **1997**, *79*, 241.
(7) Lin, E. K.; Wu, W. L.; Satija, S. K. *Macromolecules* **1997**, *30*, 7224.
(8) Hu, H. W.; Granick, S. *Science* **1992**, *258*, 1339.
(9) Keddie, J. L.; Jones, R. A. L.; Cory, R. A. *Europhys. Lett.* **1994**, *27*, 59.
(10) Keddie, J. L.; Jones, R. A. L.; Cory, R. A. *Faraday Discuss. Chem. Soc.* **1994**, *98*, 219.
(11) Forrest, J. A.; Dalnoki-Veress, K.; Dutcher, J. R. *Phys. Rev. E* **1997**, *56*, 5705.
(12) Fryer, D. S.; Peters, R. D.; Kim, E. J.; Tomaszewski, J. E.; Pablo, J. J.; Nealey, P. F.; White, C. C.; Wu, W. L. *Macromolecules* **2001**, *34*, 5627.
(13) Fryer, D. S.; Nealey, P. F.; Pablo, J. J. *Macromolecules* **2000**, *33*, 3376.
(14) Pu, Y.; Ge, S.; Rafailovich, M.; Sokolov, J.; Duan, Y.; Pearce, E.; Zaitsev, V.; Schwarz, S. *Langmuir* **2001**, *17*, 5865.
(15) Despotopoulou, M. M.; Frank, C. W.; Miller, R. D.; Rabolt, J. F. *Macromolecules* **1996**, *29*, 5797.
(16) Schönherr, H.; Frank, C. W. *Macromolecules* **2003**, *36*, 1188.
(17) Taguchi, K.; Miyaji, H.; Izumi, K.; Hoshino, A.; Miyamoto, Y.; Kokawa, R. *J. Macromol. Sci., Phys.* **2002**, *B41*, 1033.

(18) Schönherr, H.; Frank, C. W. *Macromolecules* **2003**, *36*, 1199.
(19) Despotopoulou, M. M.; Miller, R. D.; Rabolt, J. F.; Frank, C. W. *J. Polym. Sci., Polym. Phys.* **1996**, *14*, 2335.
(20) Mellbring, O.; Kihlman Øiseth, S.; Krozer, A.; Lausmaa, J.; Hjerberg, T. *Macromolecules* **2001**, *34*, 7496.
(21) Reiter, G.; Sommer, J. U. *J. Chem. Phys.* **2000**, *112*, 4376.
(22) Reiter, G.; Sommer, J. U. *J. Chem. Phys.* **2000**, *112*, 4384.
(23) Reiter, G.; Sommer, J. U. *Phys. Rev. Lett.* **1998**, *80*, 3771.
(24) Zhang, F.; Liu, J.; Huang, H.; Du, B.; He, T. *Eur. Phys. J. E* **2002**, *8*, 289.
(25) Taguchi, K.; Miyaji, H.; Izumi, K.; Hoshino, A.; Miyamoto, Y.; Kokawa, R. *Polymer* **2001**, *42*, 7443.
(26) Bartczak, Z.; Argon, A. S.; Cogen, R. E.; Kowalewski, T. *Polymer* **1999**, *40*, 2367.
(27) Sakai, Y.; Imai, M.; Kaji, K.; Tsuji, M. *Macromolecules* **1996**, *29*, 8830.
(28) Sakai, Y.; Imai, M.; Kaji, K.; Tsuji, M. *J. Cryst. Growth* **1999**, *203*, 244.
(29) Lovinger, A. J.; Cais, R. E. *Macromolecules* **1984**, *17*, 1939.
(30) Kim, J. H.; Jang, J.; Zin, W. C. *Macromol. Rapid Commun.* **2001**, *22*, 386.
(31) Schöll, A.; Fink, R.; Umbach, E.; Mitchell, G. E.; Urquhart, S. G.; Ade, H. *Chem. Phys. Lett.* **2003**, *370*, 834.
(32) Stöhr, J.; Outka, D. A.; Baberschke, K.; Arvanitis, D.; Horsley, J. A. *Phys. Rev. B* **1987**, *36*, 2976.
(33) Ge, S.; Pu, Y. K.; Zhang, W.; Rafailovich, M.; Sokolov, J.; Buenviaje, C.; Buckmaster, R.; Overney, R. M. *Phys. Rev. Lett.* **2000**, *85*, 2340.
(34) Zhang, Y.; Ge, S.; Rafailovich, M. H.; Sokolov, J. C.; Colby, R. H. *Polymer* **2003**, *44*, 3327.
(35) Johnson, K. L. *Contact Mechanics;* Cambridge University Press: Cambridge, England, 1985.
(36) Wunderlich, B. *Macromolecular Physics*; Academic Press: New York, 1973.
(37) Mandelkern, L. *Crystallization of Polymers*; McGraw-Hill: New York, 1984.
(38) Keith, H. D.; Padden, F. J. *J. Appl. Phys.* **1964**, *35*, 1270.
(39) Mayes, A. M.; Russell, T. P.; Bassereau, P.; Baker, S. M.; Smith, G. S. *Macromolecules* **1994**, *27*, 4000.
(40) Huang, J. B.; Hong, J. W.; Urban, M. W. *Polymer* **1992**, *33*, 5173. The amorphous content $x = [1 - (I_{730}/I_{720})/1.233]/(1 + I_{730}/I_{720}) \times 100$.
(41) Hagemann, H.; Snyder, R. G.; Peacock, A. J.; Mandelkern, L. *Macromolecules* **1989**, *22*, 3600.
(42) Hannay, N. B. In *Treatise on Solid State Chemistry*; Hoffman, J. D., Davis, T. G., Lauritzen, J. I., Eds.; Plenum Press: New York, Vol. 3, Chapter 7.
(43) Schonhorn, H. *Macromolecules* **1968**, *1*, 145.

MA030456B